



Optical Imaging in Oral Oncology

9

Prashanth Panta, Laurie J. Rich,
and Mukund Seshadri

Abstract

There has been widespread interest in the application of simple light-based methods and optical imaging as adjunctive tools in oral oncology. These optical imaging techniques exploit differences in properties such as absorption, reflectance, and light scattering between normal and transformed epithelium. Optical imaging methods can also utilize tissue autofluorescence arising from endogenous chromophores to detect malignant tissue. For example, early oral malignancy is often associated with a loss of fluorescence or fluorescence visualization loss (FVL) which may be used to aid in tissue selection for biopsy. The autofluorescence-based Visual Enhanced Lightscope (VELscope®), chemiluminescence-based ViziLite® system, the Identafi® system that uses multispectral fluorescence and

reflectance, and narrow band imaging (NBI) instruments are among the optical imaging-based diagnostic platforms that are currently available for clinical use. In addition, photoacoustic imaging (PAI) is an advanced hybrid imaging method that allows for deep tissue imaging and is actively being evaluated for diagnostic applications in oncology. In this chapter, we will review the basics of these optical imaging methods and summarize pre-clinical and clinical evidence on their performance in oral oncology. The goal of this chapter is to provide the reader with an overview of these methods and their potential clinical applications.

9.1 Introduction to Light-Based Methods

Reliable identification of oral cancer and precancer cannot be based on visual examination alone since the human eye is not optimized to detect disease based on tissue contrast [1]. However, spectral differences between normal and diseased tissue can be visualized through the use of optical imaging methods that can improve our visual perception. These optical methods can exploit differences in optical properties of tissues such as fluorescence, reflectance, and chemiluminescence.

P. Panta, MDS (✉)
Department of Oral Medicine and Radiology,
MNR Dental College and Hospital,
Sangareddy, Telangana, India
e-mail: maithreya.prashanth@gmail.com

L. J. Rich, PhD · M. Seshadri, DDS, PhD
Department of Oral Oncology,
Roswell Park Comprehensive Cancer Center,
Buffalo, NY, USA
e-mail: laurie.rich@roswellpark.org;
Mukund.Seshadri@roswellpark.org

9.2 Tissue Fluorescence or Autofluorescence

Cells and tissues in the body contain molecules which have the ability to “fluoresce” (i.e., glow) when excited by light of specific wavelength. When a tissue is illuminated with light of short wavelength (for example, blue light), cells become excited and emit light that is of a longer wavelength (low energy). Importantly, while normal cells emit green light, abnormal cells do not emit light. Exposure to blue light spectra (400–460 nm) may maximize a differential profile in areas undergoing neoplastic change [2]. This fluorescent signal arises from naturally occurring compounds in tissues called chromophores or fluorophores. Fluorophores are molecules that absorb light at one wavelength and emit light at longer wavelength [3]. The main fluorophores capable of fluorescence in the 400–460 nm range are nicotinamide adenine dinucleotide (NADH) and flavin adenine dinucleotide (FAD), cellular coenzymes, collagen, and elastin in connective tissue. Hemoglobin (in blood) also absorbs light and results in loss of fluorescence in regions with high concentration. Other endogenous fluorophores include structural proteins and amino acids. Each fluorophore has a unique excitation spectrum, allowing for multispectral assessment of specific fluorophores. For example, increased metabolism typically observed in cancer changes FAD levels [4]. Scattering is another mechanism of fluorescent visualization that is influenced by tissue keratinization status, epithelial thickening of oral mucosa, and by nuclear scatter at the cellular level. The degree of keratinization varies from individual to individual and is also site-specific. For example, the tongue and buccal and alveolar mucosa are covered by keratinized epithelium, while the floor of mouth is nonkeratinized. A greater nuclear scatter can result from the high nuclear-to-cytoplasmic ratio in dysplastic tissues. This is especially true for amelanotic epithelial tumors like OSCC [5]. The scatter cross section (μm^2) in dysplastic nuclei ($80 \mu\text{m}^2$) is approximately four times greater than a normal cell ($20 \mu\text{m}^2$) at the same wavelength [5, 6]. At

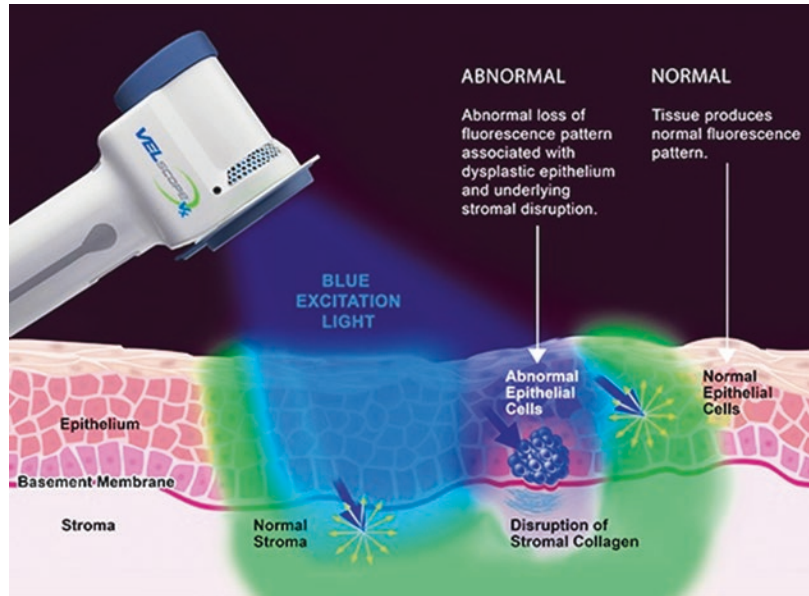
Table 9.1 Mechanisms behind loss of fluorescence

Mechanism	Reasons	
Increased absorption	Absorption of light by hemoglobin and other absorbers.	
Decreased emission	By chromophores: NADH, FAD, collagen, elastin etc.	
Increased scatter	Cell level	Cellular nuclei contribute to scatter
	Tissue level	Keratin, thick epithelium, and stromal collagen contribute to scatter

the fundamental level, fluorescence visualization is dependent on the absorption of light by certain absorbers, and emission of fluorescent light by naturally occurring tissue fluorophores, in addition to scattering caused by thick keratin blanket covering tissues [3] (Table 9.1).

Malignant transformation results in cellular changes such as increased nuclear-to-cytoplasmic ratio, nuclear clumping, pleomorphism and changes in epithelium, and alterations in stromal architecture. The breakdown of collagen in the extracellular matrix and break in basement membrane also contribute to the loss of tissue fluorescence [7]. Studies have shown significant changes in stromal biology during the evolution of oral precancer [8]. The volume fraction of collagen fibers in supporting stroma decreases with the progression of disease [5]. In tissue stroma, collagen fibers are the main light scatterers. Collagen by nature has high refractive index, and hence scattering of light in the stroma is higher than the scattering in the epithelium. The hallmark autofluorescence and reflectance signals in oral malignancy are primarily due to changes in the underlying connective tissue. During malignant progression, several enzymes (proteases, etc.) mediate the invasion of tumor into connective tissue, destroying collagenous stromal architecture. As a result, the collagen fibers are broken down, and their arrangement becomes disorganized and more detached with a tendency to aggregate [5]. The gap created between collagen fibers due to this breakdown adds to contrast and represents a constant intensity region. This arrangement of collagen fibers can be validated using confocal microscopy. The identification of subtle changes

Fig. 9.1 Appearance of normal and abnormal mucosa under VELscope® tissue fluorescence imaging (courtesy of LED Dental, Inc.)



in connective tissue is therefore possible with autofluorescence-based optical methods and scattering-based methods such as optical coherence tomography. Loss of fluorescence or fluorescence visualization loss (FVL) was also used in the detection and mapping of field changes in oral malignant and potentially malignant disorders [9]. FVL was noticed in all 20 tumors and was extending far away (25 mm) from the clinically visible lesion (subclinical extension). In the study, 32 of 36 (~89%) FVL-guided biopsies showed histological change ranging from low-grade dysplasia to squamous cell carcinoma [9]. All 36 biopsies showed either histological change and/or genetic alteration. The FVL-guided margin biopsies in oral tumors with low-grade dysplasia or no dysplasia revealed loss of heterozygosity at 3p and/or 9p, a molecular change associated with high recurrence [9].

VELscope® (Visual Enhanced Light scope) is now a widely used handheld optical device for oral cancer screening that uses autofluorescence technology. It is an approved visual enhancement system compatible for use as an adjuvant tool for oral assessment in combination with routine oral examination. The VELscope® device utilizes blue light excitation between 400 and 460 nm to

visualize the abnormality of the oral cavity by the property of direct tissue autofluorescence. The normal oral mucous membrane demonstrates a pale green fluorescence on absorption of blue light emitted by the device (Fig. 9.1). Abnormal tissue (i.e., tissue with dysplasia or malignancy) presents as a dark region due to loss of autofluorescence, a property natural to healthy tissues. Fluorescence visualization loss (FVL) is the hallmark of neoplastic process. The VELscope® device exploits this biological characteristic to distinguish healthy tissues or benign lesions from dysplastic tissue. In inflammatory lesions, this device shows false positives mainly due to the elevated blood flow and concentration of hemoglobin, which is a natural chromophore that absorbs light resulting in FVL [10].

It takes ~2 min for complete visualization and is hence an easy-to-use clinical device. Newer generation devices also possess an imaging adapter compatible with a mobile device for case documentation. The device now has a single-use lens cap to prevent cross contamination between patients. Lesions that are positive on VELscope® examination are suggested to be observed for 2 weeks for resolution, or else biopsy is recommended [11].

9.3 Chemiluminescence

The technique of chemiluminescence was first applied in the detection of cervical dysplasia. ViziLite® is the popular device that employs the principle of chemiluminescence developed by Zila Pharmaceuticals (Phoenix, AZ). In 2001, it received FDA clearance. This technology is utilized in gynecology, where it was termed as “speculoscopy” and is followed by thorough cervical examination [12]. Commercial chemiluminescence devices are either peroxyoxalate or luminol based systems. Three commercially available devices operate with the working principle of chemiluminescence for detection of oral cancer. They include ViziLite®, ViziLite Plus®, and Microlux/DL™. In the oral cancer setting, chemiluminescence was shown to be superior to toluidine chloride [13]. The specificity of ViziLite® was poor, but accuracy was 80%. They (ViziLite® and ViziLite Plus®) were able to improve brightness, sharpness, texture, and size of the lesion [14, 15]. This technique is entirely based on reflectance of oral tissue as a result of the increased nuclear-cytoplasmic ratio.

The examination is done in a dim lighted room to facilitate lesion recognition. It is best to photograph the observations made by ViziLite® for documentation purposes. The ViziLite® kit has (a) 1.1% acetic acid rinse; (b) capsule which contains sodium benzoate, propylene glycol, and alcohol base; and (c) retractor. Once activated, the glass vial containing hydrogen peroxide breaks and reacts with acetylsalicylic acid (aspirin). The energy liberated in this reaction is absorbed by a fluorescent dye to convert it into white light. In the chemiluminescence system, a light of specific wavelength is emitted from a reaction between hydrogen peroxide and acetylsalicylic acid inside a light stick [16]. The reaction produces blue light at the desired wavelength for exposure of oral tissues. It involves the use of an oral rinse of acetic acid (1%) for 1 minute followed by examination of oral mucosa under diffuse chemiluminescent low-energy blue/white light at a wavelength of 490–510 nm. The chemiluminescence test has an acetic acid prerinse step to remove debris and glycoprotein coat that

limits passage of light through tissue. Acetic acid desiccates the tissue, coagulates, and precipitates proteins on the epithelial surface. The majority of potentially malignant disorders (75%) were aceto-white. The theory behind this observation is that acetic acid removes glycoprotein and slightly desiccates the oral mucosa. Hence, the normal mucosa will appear blue, while the abnormal mucosa will reflect light due to high nuclear-cytoplasmic ratio. Furthermore, abnormal mucosa appears more aceto-white and brighter, with sharper and more distinct margins. In a typical exam, the occurrence of acetowhite staining is considered as “positive,” and the absence of acetowhiteness is considered as “negative.”

Recently, the ViziLite® system was modified to include toluidine blue (ViziLite Plus®-toluidine blue system). The major disadvantage with ViziLite® kit is that it is a single-use product. The ViziLite Plus® kit consists of swab components with 1% acetic acid rinse, toluidine blue, and a decolorizer [12]. The toluidine blue in ViziLite Plus® improves the visualization by chemiluminescence. In a large patient cohort, leukoplakias were more significantly aceto-white than erythroplakia [17]. In a study comparing efficacy of chemiluminescent light, toluidine blue and exfoliative cytology, the chemiluminescent test was shown to generate reliable results [18]. Several studies have shown high sensitivity with ViziLite Plus®, although low specificity was the main limitation [15–18]. Identification and delineation of dysplasia is challenging, but potentially malignant lesions can be easily identified. In summary, the ViziLite Plus® chemiluminescence system can be used as a supplementary investigation following routine oral examination to improve identification of oral abnormalities [17].

Microlux/DL™ is a battery-operated device with comparable efficacy to ViziLite® and ViziLite Plus® [19]. Microlux/DL™ was shown to enhance clinical visibility, but could not uncover clinically invisible lesions. The overall sensitivity and specificity were 77.8% and 70.7%, respectively [19]. Adding toluidine blue did not increase the efficacy of Microlux/DL™ [20]. Further studies are needed on the efficacy of Microlux/DL™.

9.4 Multispectral Fluorescence-Reflectance Imaging

Identafi® 3000 is the most recent of commercially available optical devices for detection of oral cancer. The system utilizes multispectral fluorescence and reflection technology to enhance visualization of mucosal abnormalities. This small, cordless, handheld device, similar to a dental airtor, offers a three-wavelength optical illumination and visualization system. Identafi® 3000 uses white, violet, and green-amber wavelengths of light which excite the oral tissues. Reusable eye wear is available which enhances contrast and visual effect and allows transmission of reflected light. In the first stage, concentrated white light is used for a thorough oral examination. The clinician then switches to violet to make second observation. Violet light (405 nm) excites oral tissues that exhibit intrinsic fluorescence. Suspected lesions do not exhibit fluorescence and therefore appear dark. There is sufficient evidence that violet light can differentiate normal and cancerous tissue with high sensitivity and specificity [8, 21]. When an abnormality is suspected, the clinician switches to green-amber light (540–575 nm), which enhances the tissue's reflectance to allow the clinician to directly observe the tissue vascularity [22], which can be used to make a tentative diagnosis. In the normal mucosa, the vasculature is clearly defined, while malignant or OPMDs exhibit dilated and diffuse vascular architecture that is more diffuse. This multispectral light system gives more visual information to the clinician, supporting decision-making on suitable management [23].

Identafi® 3000 has been shown to exhibit high sensitivity (82%) and specificity (87%) in differentiating neoplastic from nonneoplastic tissue [24]. The degree of vascularity observed using the system has been shown to correlate with expression of CD34 in histological sections [22]. Overall, 66% agreement was observed between clinical and histological grade [22]. The increase in vascularity was not limited to carcinomas, but even simple leukoplakias, hyperkeratotic lesions and lichen planus have demonstrated increased vascularity. Patients with severe clinical (green-amber light visualization) and histological grade

of vascularity may be kept for future follow-up, but this consideration needs validation.

9.5 Narrow Band Imaging

Generally, endoscope-connected narrow band imaging (NBI) systems are useful in the visualization of the posterior oral cavity (oropharynx) not accessible during routine oral examination. In the past, it was applied mainly to the larynx, esophagus, stomach, and colon. The extensive work of Yang et al. [25–29] has provided foundational evidence on the use of NBI in oral malignant lesions and potentially malignant disorders and has shown specific in vivo application [30, 31]. NBI has been used in the identification of high-grade dysplasia/carcinoma in oral erythroplakia [31]. Ottaviani et al., have shown that NBI can also be used tumor angiogenesis [32]. In a more recent meta-analysis by Zhou et al. on head and neck cancer which included 6187 lesions, the overall area under the summary receiver operating characteristic (SROC) curve was 96.94% and for oral and oropharyngeal cancers (1071 lesions), the area under the SROC curve was 94.53% [33].

9.5.1 Principle

Endoscope-guided NBI enhances the visualization of oral tissue through the magnification of mucosal texture and vascularity. As a result, NBI provides more information than broadband white light images. In NBI, white light is filtered to produce two narrow bands (~30 nm) of blue and green light (Fig. 9.2a) [34]. The blue band (415 nm) corresponds to the Soret absorption peak of hemoglobin, and the green band (540 nm) supports the visualization of underlying vasculature [34, 35] (Fig. 9.2b). Imaging at the blue wavelength reveals superficial, fine vasculature, while the green wavelength light reveals deeper vessels with large diameter (Fig. 9.2c). In normal tissues, the capillaries in connective tissue below the epithelium are visible because many regions of the oral mucosa are free of appendages, except for the minor salivary glands. Capillaries in the floor of mouth, lip, and buccal mucosa are more

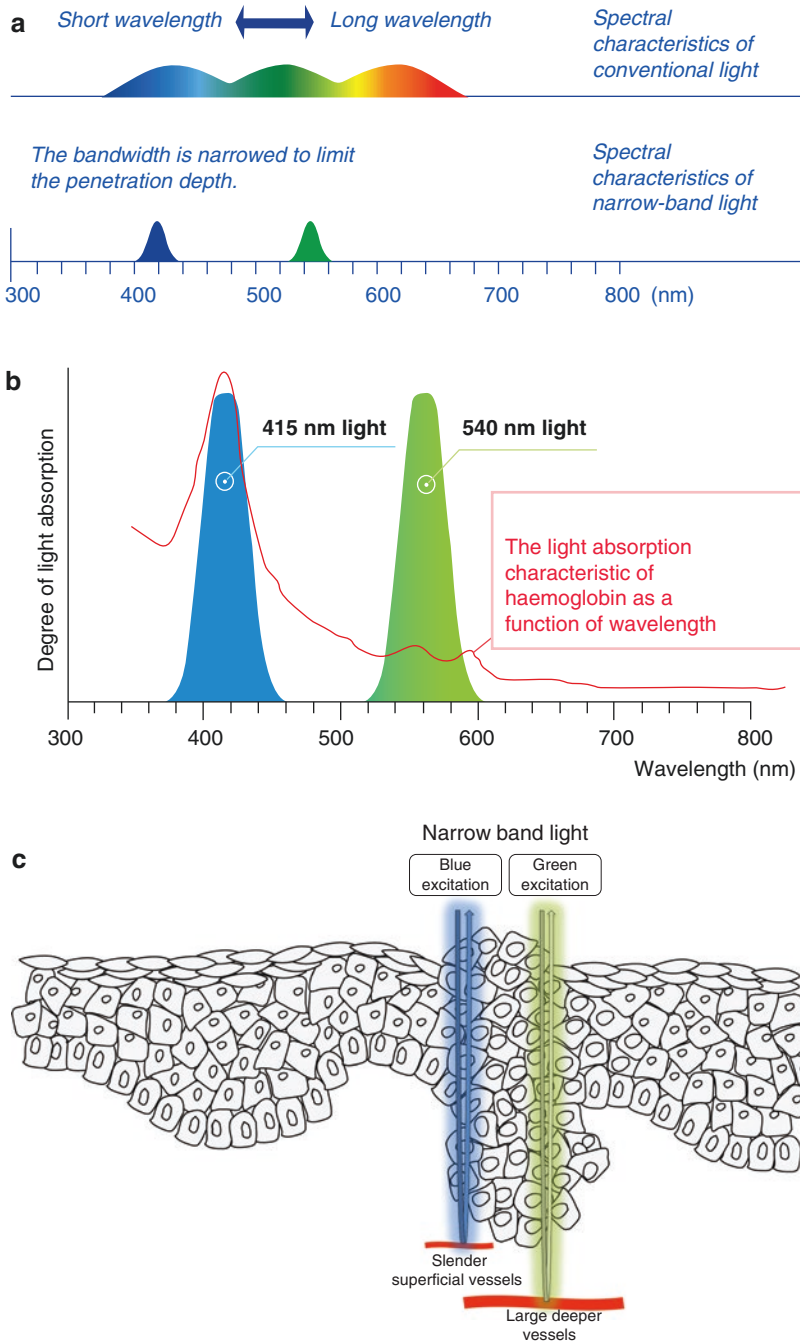


Fig. 9.2 Panel (a): Spectral characteristics of conventional white light, and narrow band light is blue-green spectrum; Panel (b): the absorptive characteristics of hemoglobin which falls within the blue and green spectrum; Panel (c): Illumination of visible light in narrow wavelength band (centered on blue and green spectrum).

The absorption and reflectance gives a neat picture of the underlying vasculature as it contains hemoglobin, the major endogenous chromophores. The distribution of slender peripheral vessels and larger deep submucosal veins is distinctive. (a and b courtesy of Olympus)

prominent than capillaries at other locations like the ventral tongue [36]. The rete pegs and connective tissue papilla are closely connected and intact, forming uniform loops. In cancer, when the association between rete pegs and underlying connective tissue is lost, the homogenous arrangement of microvasculature in tissue is disrupted. In advanced cancers, the high growth rate of capillaries may be also visualized as discolored areas or spotting of tissue. Based on the pattern of tumor growth (inward or outward), this architecture and organization of vessels is disturbed leading to an irregular pattern. At the tissue level, three phenomena occur in and around transformed tissue which are detectable by NBI: (i) vascularization due to tumor angiogenesis, (ii) vascular destruction due to uncontrolled proliferation, and (iii) displacement of existing vasculature leading to irregular vessel pattern or discolored appearance of cancer tissue [36]. NBI is based on the intrapapillary capillary loops (IPCL), and microvascular morphology detected by narrow band imaging (NBI) can assist in diagnosis. Normal mucosa shows regular looping in uniform pattern (Type I), nonneoplastic lesions show mild change in morphology (Type II, Type III), and neoplastic lesions show irregular pattern with several loop shapes (Type III, Type IV) [37] (Table 9.2). In NBI, the severity of OSCC as measured by tumor size, nodal status, TNM stage, lymphovascular or perineural invasion, depth of tumor infiltration, and

tumor differentiation was associated with specific morphological patterns in intrapapillary microvasculature, with PCL destruction from tumor angiogenesis being associated with more advanced disease stage [38]. Takano et al. have demonstrated the value of NBI as a potential tool for the detection of early cancer, and microvascular organization is a dependable biomarker of oral cancer [37]. A narrow band image of high-grade dysplasia and oral cancer shows increased number of tortuous, dilated, twisted, elongated, and corkscrew vessel morphology (Fig. 9.3) [31]. Elongated, twisted, and destructive pattern are indicators of dysplasia, carcinoma in situ, and invasive carcinoma arising in ‘erythroplakia’ [31].

NBI is a safe, noninvasive endoscopic imaging method for detailed viewing of oral cancer, oral leukoplakia, and erythroplakia [29, 36, 37]. NBI has also been used in the identification of squamous cell carcinoma arising in nonhealing ulcers [36]. Furthermore, NBI is capable of evaluating microvascular organization and provides clear images for simplified clinical decision-making. Understanding the intrapapillary capillary loops (IPCL) during oral carcinogenesis could potentially enhance the clinical utility of NBI [37, 38]. Changes in IPCL have been previously correlated with invasion depth of esophageal SCC and histological atypia [39]. IPCL patterns have also been correlated with increased severity in leukoplakia [29]. Additionally, IPCL was the only independent factor associated with the occurrence of squamous cell carcinoma in oral chronic nonhealing ulcers [36]. Some individuals with early cancer also presented with brown coloration on NBI [36, 37]. Future studies should continue to focus on the identification and characterization of specific microvascular patterns relating to different stages in the evolution of cancer and molecular parameters [34]. A multispectral digital microscope was recently developed which creates images in narrow band, fluorescence, and orthogonal polarized reflectance mode [35]. NBI has also been applied in robotic-guided surgical procedures in HNSCC for identification of margin dysplasia to obtain safe surgical margins in anatomically challenging areas to minimize morbidity and functional preservation of normal tissue.

Table 9.2 Comparison of IPCL patterns in suspicious oral lesions

Type I	Regular brown dots	<ul style="list-style-type: none"> • Normal mucosa • Homogenous 	Low risk IPCL pattern
Type II	Dilation and crossing	<ul style="list-style-type: none"> • Leukoplakia • Squamous hyperplasia 	
Type III	Elongated and meandering	<ul style="list-style-type: none"> • High-grade dysplasia • Carcinoma in situ 	High risk IPCL pattern
Type IV	Destruction and angiogenesis	<ul style="list-style-type: none"> • Carcinoma in leukoplakia • Carcinoma in erythroplakia • Carcinoma in non-healing ulcers 	

IPCL patterns advance with increasing severity of pathology; the destructive pattern is associated with the most advanced carcinomas (classification of Takano et al. [37] and IPCL correlation adapted from Yang et al. [25–29, 31, 38])

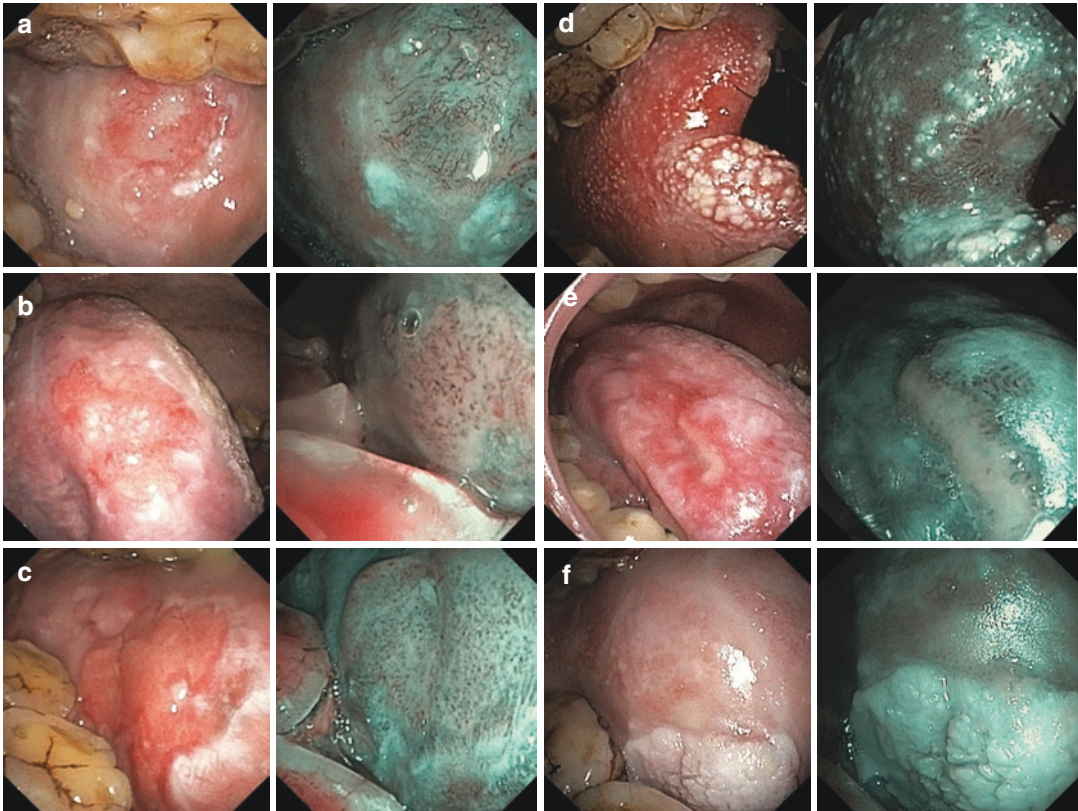


Fig. 9.3 Suspicious oral lesions under NBI light showing different IPCL vessel patterns. (a) Dilatation, meandering of capillaries (intramucosal cancer); (b) dilatation, meandering, calibre change, nonuniformity of intrapapillary capillary loop (intramucosal cancer); (c) uniform small dots in submucosally (carcinoma in situ); (d) thin capillar-

ies uniformly distributed between white spotted lesion (inflammatory pathology-hyperplastic candidiasis); (e) inflammatory base with uniformly distributed capillaries in submucosal plane; (f) hyperkeratotic lesion (“umbrella effect”) without surrounding mucosal changes (homogeneous leukoplakia) (courtesy of Rakesh Srivastava, India)

9.6 Quest for Deep Tissue Imaging

Light-based systems exploit tissue features like epithelial thickness, blood vessel pattern (vasculature), and cellular features like nuclear-cytoplasmic ratio to generate structural and functional information on these tissues. Alterations of these tissue characteristics can therefore be exploited to differentiate normal tissues from those that have undergone or are undergoing malignant transformation [23].

There is some contradicting evidence on the role of light-based detection methods for oral cancer screening [40]. The scope of optical tools in diagnosis has increased due to their ease of use, short image acquisition times, and lower cost compared to traditional radiologic techniques such as PET or CT. Furthermore, these noninvasive optical imaging methods are patient-friendly (less intimidating or claustrophobic) and offer the ability to provide structural and functional information in real time. Moreover, optical imaging can be repeated frequently

without risk of exposure to ionizing radiation or radioactive tracers [23]. However, depth of penetration is a limitation for most optical methods (in the order of millimeters) that contributes to inadequate visualization of subsurface layers in tomographic sections. Increased scattering of light with increasing depth is the primary limitation of traditional ballistic optical imaging methods which restricts imaging depths to a few millimeters. In this regard, photoacoustic imaging (PAI) is a hybrid optical and ultrasound imaging method that exploits optical properties of tissue to provide molecular information of tissue at imaging depths typically associated with ultrasound. The following section describes the potential of this emerging advanced optical imaging method since it is currently not readily available for clinical application but has strong potential as a chairside tool in the near future. However, it is important to remember that all optical techniques are ultimately intended to serve as adjuvant aids that compliment clinical assessment.

9.7 Photoacoustic Imaging

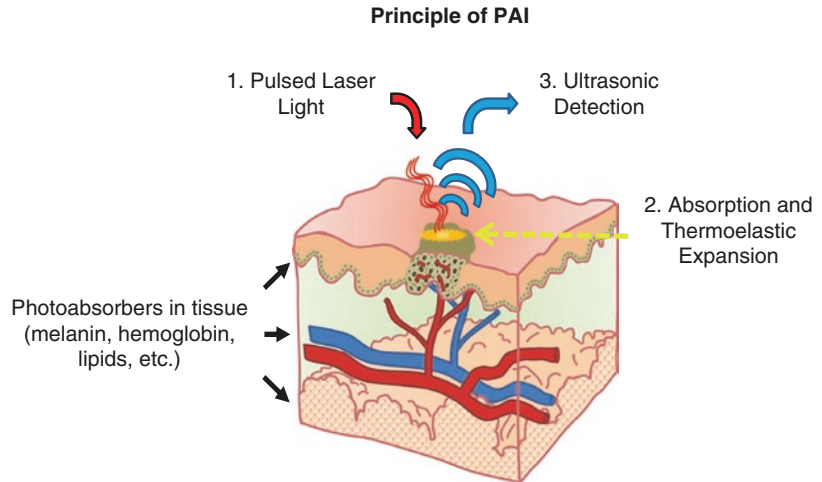
PAI is a hybrid imaging technique that combines optics and ultrasound (US) and is based on the photoacoustic effect [41]. The photoacoustic effect was first explored by Alexander Graham Bell [42] and is a phenomenon wherein light is absorbed by photoabsorbers within a medium resulting in a localized thermoelastic expansion, producing pressure waves that can be acoustically detected [42]. It took 100 years to evolve as a biomedical imaging technique (1981) based on fundamental work by Dr. Theodore Bowen [43–45]. However, it was not until the 1990s that PAI was developed for imaging in tissues, pioneered by Dr. Robert Kruger [46, 47]. Similar to conventional optical techniques, PAI can detect endogenous chromophores through multispectral excitation and detection of the unique absorption profile of each chromophore [48]. In this manner, PAI can provide important molecular information of tissue at clinically relevant imaging depths (on the order of several centimeters).

9.7.1 Principle

PAI can be considered an ultrasound-based imaging method with light-generated contrast. The generation of PA signal relies on three steps (Fig. 9.4): (1) deposition of electromagnetic energy (EM) into the tissue being imaged, (2) absorption of the EM energy by photoabsorbers within tissue, and (3) thermal expansion of optical species in tissue to release pressure waves detectable by US [48, 49]. Whereas traditional optical imaging techniques are limited to 2–3 mm due to relatively high scattering of light in tissue, tissues show low acoustic scattering (1/1000 times less than optical scattering) allowing for significantly improved imaging depths in the order of centimeters [48].

Contrast in PAI is influenced by the optical absorption coefficient and concentration of photoabsorbers in each tissue type [50, 51]. PAI works optimally on tissues with high optical coefficients like blood vessels which contain high levels of hemoglobin [52]. PAI can also be performed at longer infrared wavelengths as it is not as rapidly absorbed by tissue and can therefore penetrate deep in tissue [50]. The main optical absorbers and generators of photoacoustic signal in tissue are hemoglobin, melanin, lipids, and water [53]. In vivo photoacoustic signal that returns from these endogenous species in tissue can be used to obtain structural and functional information including vascular hemodynamics, hemoglobin concentration, oxygen saturation, and tissue composition of photoabsorbers [53]. Image reconstruction allows for the localization of photoabsorbers within tissue through time and amplitude-based detection of PA signal. In the majority of commercially available PAI systems, the light source and ultrasonic detector are incorporated together into a single transducer for more efficient work flow. The two most common PAI systems utilize either a ring/bowl array where piezoelectric elements are positioned around the tissue being imaged or a linear array where piezoelectric elements line the face of the image probe [48, 49]. In the first design, generated PA signal is detected at multiple positions around the tissue and then back-projected to determine the original

Fig. 9.4 Principles of PA signal generation. Light is pulsed into tissue (1) where it is absorbed by photoabsorbers (2), resulting in pressure waves that can be detected by ultrasound (3)



source of the PA signal, similar to reconstruction methods used for x-ray computed tomography [51]. The second design functions similar to standard ultrasound where the generated PA signal is detected by individual elements along the axis of the probe corresponding to a specific image segment [54]. In this method, the light pulse is synchronized with the image acquisition time to allow for accurate spatial localization of the photoabsorber. Photoabsorber depth is then estimated by measuring the time of PA signal arrival. While tomographic techniques can provide greater sensitivity and resolution compared to that of linear array techniques, linear array techniques readily allow for simultaneous PAI and US enabling structural, functional, and molecular imaging of tissue [55–58].

9.7.2 Contrast Agents in PAI

9.7.2.1 Endogenous Contrast Mechanisms

In oral cancer, angiogenesis and hypoxia are a fundamental process, and their grade increases with severity of malignancy [59, 60]. Consequently, PA-based assessment of tissue hemoglobin and oxygenation could assist in the diagnosis and staging of oral lesions. Early work by Oraevsky and colleagues highlighted the potential of PAI for detecting DMBA-induced oral lesions in the hamster buccal

pouch carcinoma model [61, 62]. In the same model, Fatakdwala et al. evaluated the ability of PAI to detect both precancerous and cancerous lesions within the oral cavity [63]. PAI detected high vascular density in oral lesions compared to normal oral mucosa associated with increased angiogenesis. Furthermore, they were able to detect increased accumulation of mucin, a key component of mucus, in precancerous lesions. In ex vivo thyroid tissue specimens, Dogra et al. found that malignant samples had significantly higher deoxyhemoglobin levels than both benign and normal thyroid tissue samples, indicating that the oxygenation status of suspicious lesions can also be used to identify malignant tissues [64]. A recent study evaluating the ability of PAI to differentiate malignant and benign thyroid nodules in vivo found that malignant lesions had higher PA signals at 760, 850, 930, and 950 nm wavelengths [65]. Multiple studies in preclinical models of oral and head and neck cancers have also highlighted the potential of PAI for tumor oxygenation kinetics and response to chemotherapy and radiation [66, 67]. These studies have demonstrated that PAI can be effectively utilized for frequent and repeated assessment of tumor oxygenation before, during, and after radiation therapy (RT) [67]. Recent work has also revealed the potential of PAI based biomarkers of oxygenation as early indicators of therapeutic efficacy [67, 68].

9.7.2.2 Exogenous Contrast Agents

While the ability of PAI to detect endogenous chromophores is a major strength of the technique, exogenous contrast agents can also be utilized to enhance contrast and signal-to-noise (SNR) in PAI [69–71]. Several classes of agents ranging from near-infrared optical dyes such as indocyanine green (ICG), metal or semiconducting nanoparticles such as gold or silver nanorods, and organic nanostructures such as chimeric polypeptide nanoparticles have been studied for their utility as contrast agents for PAI [70]. These agents can be administered as neat solutions without targeting moieties to measure vascular parameters, or with targeting ligands to visualize molecular processes.

Recently, nanostructures prepared from gold and silver have been used as exogenous contrast agents for PAI [72]. The advantage of gold nanoparticles is their strong optical absorption due to their high cross section tuned to the optical window (~730 nm). This minimizes PA signal from endogenous absorption while maximizing imaging depth [41]. These metallic nanoparticles have a fivefold to ninefold higher optical absorption due to surface plasmon resonance (SPR), the property by which incident light excites the outer electrons in metals producing oscillations of conducting electrons [73]. SPR structures used for PAI include gold nanoclusters, gold nanospheres,

gold nanorods, gold nanoshells, gold cages, and silver nanoplates [72]. Injection and accumulation of these agents in tumors produces increased PA signal associated with tumor angiogenesis and vascular perfusion [73]. Consequently, these agents have been used for selective identification of tumors from non-tumor tissue [74] and to assess temporal and spatial changes in PA signal corresponding to areas of high vascular perfusion [75]. In head and neck tumor models, PAI has been shown to detect differential uptake of EGFR and human epidermal growth factor receptor 2 (HER2) targeted gold nanorods, highlighting the potential of PAI for molecular profiling of tumors and treatment planning of OSCC patients [76]. In addition to standard PEGylated metallic nanoparticles, silica coated hybrid particles show stable and improved PAI signal [77, 78]. A threefold enhancement in PA signal was seen in silica-coated gold rods [78]. However, biodegradable nanoparticles are preferable as metallic particles pose risk of toxicity due to accumulation.

PAI studies have also utilized NIR absorbing dyes (methylene blue, indocyanine green) to enhance PAI contrast as they are inexpensive, widely available, and approved for clinical use (Figs. 9.5 and 9.6) [76]. Their structure is typically comprised of a series of conjugated double bonds in ring system which lowers the energy necessary for excitation [77]. The two US Food

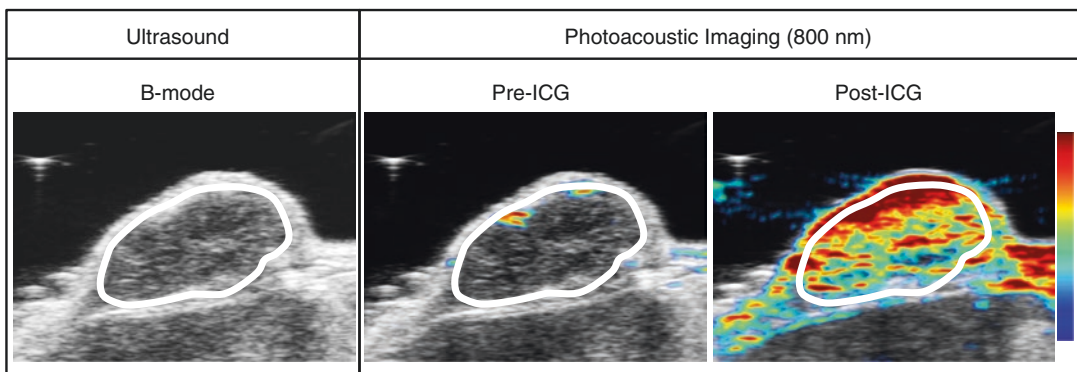


Fig. 9.5 Enhancement of photoacoustic imaging signal using an exogenous dye. (Left) B-mode ultrasound image shows presence of subcutaneous patient derived head and neck tumor xenograft (white outline) grown in a severe combined immunodeficient mouse. (Right) Photoacoustic

signal intensity maps (800 nm) acquired before and immediately following injection of 2 mM indocyanine green (ICG) dye (200 μ l). Following injection, vascularized areas show a noticeable increase in photoacoustic signal (areas of red)

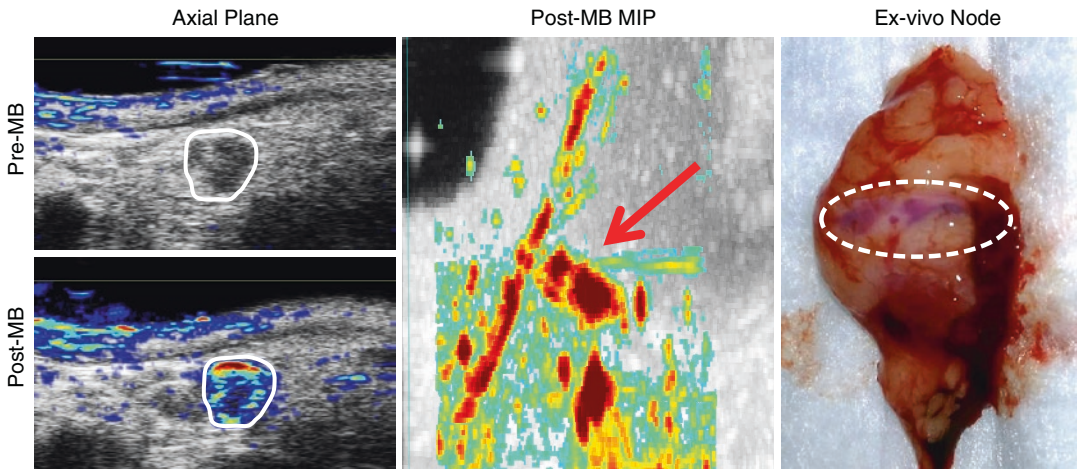


Fig. 9.6 Photoacoustic lymphangiography of a draining lymph node in a New Zealand white rabbit. (Left) Photoacoustic signal intensity maps (680 nm) of the parotid lymph nodes before and immediately following injection of 1% methylene blue (MB) dye in the rabbit ear. (Middle)

Maximum intensity projection (MIP) showing the draining lymph vessel tract and accumulated dye in the parotid lymph node (red arrow). (Right) Ex vivo white light image of the rabbit parotid gland removed following imaging shows dye accumulating in the node (white circle)

and Drug Administration-approved dyes, indocyanine green (ICG) and methylene blue, can also serve as effective contrast agents for PAI of tumors and tumor-draining lymph nodes (Fig. 9.6). Studies have demonstrated the potential of PA-guided tumor lymphangiography for mapping of sentinel lymph nodes [79, 80]. Porphyrins are also organic compounds that are highly tunable and have intense absorptive properties allowing for PAI [81]. Using porphyrin nanoparticles, Muhanna and colleagues used PAI prior to photothermal therapy to measure the drug uptake levels in the VX2 carcinoma model of invasive OSCC, showing that PAI can be used to guide cancer therapies to improve treatment efficacy [82]. Targeting moieties have also been added to optical dyes to increase their tumor specificity and to identify molecular processes. Using a novel caspase-9 near-infrared PAI probe, Yang et al. were able to detect increased contrast uptake in tumors 24 h after treatment with cisplatin [83].

Luke et al. used PAI to detect metastatic cervical lymph nodes in mice bearing FaDu tumors of the tongue, by measuring the uptake of EGFR-targeted molecularly activated plasmonic nanosensors following peritumoral injection [84].

Importantly, their method provided a sensitivity and specificity of 100% and 87.5% compared to 50% and 87% of current PET methods. The ability of PAI to detect metastatic lesions was also assessed using a VX2 carcinoma large animal model of invasive OSCC, where dual PA and fluorescent nanoparticles were injected into the peritumoral space and used to guide surgical resection of tumor-draining lymph nodes [85]. Luke et al. also showed that it was possible to detect metastatic nodes without the need for exogenous contrast as metastatic lymph nodes had significantly lower %sO₂ levels than healthy nodes, although their sensitivity and specificity was reduced to 71% and 83%, respectively [86]. This is a considerable advantage over conventional lymphangiography methods as it would not require the administration of exogenous agents for the detection of sentinel lymph nodes.

In summary, PAI has the potential to become a simple dental chairside or bedside imaging tool for the diagnosis and staging of oral cancer. The development of compact PAI systems with co-registered US could facilitate widespread clinical utilization of this promising imaging modality. Enhancing PAI signal using exogenous agents can significantly improve PAIs' ability to detect

and characterize oral lesions and could have a role for treatment planning and therapeutic response monitoring.

Conclusion

Optical imaging methods can probe the tissue architectural, cellular, biochemical, and metabolic landscape in oral cancer. Given their ease of use, a number of optical imaging methods have been studied for clinical applications in oral oncology. Tissue architectural changes in precancerous and cancerous tissues affect their optical properties and can be visualized using autofluorescence, chemiluminescence, multispectral fluorescence, and narrow band imaging methods. Optical and optoacoustic imaging methods using exogenously administered optical contrast agents for cancer diagnosis have also shown promise. Combined or multimodal application of these optical techniques can improve their diagnostic utility. However, the optical imaging methods can only serve as adjuvant tools. The findings from using these aids should always be interpreted in the context of clinical examination and are often useful when performed by skilled and experienced clinicians. Future developments in hardware and improved algorithms could improve their overall diagnostic power and enable creation of cheap, easy-to-use, and reliable tools for in vivo visualization of oral cancer and precancer.

Acknowledgments Support from R01CA204636, R01DE024595, S10OD010393-01, and P30CA06156 is gratefully acknowledged.

References

1. Utzinger U, Bueeler M, Oh S, Heintzelman DL, Svistun ES, Abd-El-Barr M, et al. Optimal visual perception and detection of oral cavity neoplasia. *IEEE Trans Biomed Eng.* 2003;50:396–9.
2. Lane PM, Gilhuly T, Whitehead P, Zeng H, Poh CF, Ng S, et al. Simple device for the direct visualization of oral-cavity tissue fluorescence. *J Biomed Opt.* 2006;11:024006.
3. Laronde DM, Williams PM, Hislop TG, Poh C, Ng S, Bajdik C, et al. Influence of fluorescence on screening decisions for oral mucosal lesions in community dental practices. *J OralPathol Med.* 2014;43:7–13.
4. Skala MC, Riching KM, Gendron-Fitzpatrick A, Eickhoff J, Eliceiri KW, White JG, et al. In vivo multiphoton microscopy of NADH and FAD redox states, fluorescence lifetimes, and cellular morphology in precancerous epithelia. *Proc Natl Acad Sci U S A.* 2007;104:19494–9. Epub 2007 Nov 27
5. Arifler D, Pavlova I, Gillenwater A, Richards-Kortum R. Light scattering from collagen Fiber networks: micro-optical properties of normal and neoplastic Stroma. *Biophys J.* 2007;92:3260–74.
6. Pavlova I, Weber CR, Schwarz RA, Williams MD, Gillenwater AM, Richards-Kortum R. Fluorescence spectroscopy of oral tissue: Monte Carlo modeling with site-specific tissue properties. *J Biomed Opt.* 2009;14:014009.
7. Pavlova I, Williams M, El-Naggar A, Richards-Kortum R, Gillenwater A. Understanding the biological basis of autofluorescence imaging for oral cancer detection: high-resolution fluorescence microscopy in viable tissue. *Clin Cancer Res.* 2008;14:2396–404.
8. Lane P, Lam S, Follen M, MacAulay C. Oral fluorescence imaging using 405-nm excitation, aiding the discrimination of cancers and precancers by identifying changes in collagen and elastic breakdown and neovascularization in the underlying stroma. *Gen Med.* 2012; 9: S78–82.e1–8.
9. Poh CF, Zhang L, Anderson DW, Durham JS, Williams PM, Priddy RW, et al. Fluorescence visualization detection of field alterations in tumor margins of oral cancer patients. *Clin Cancer Res.* 2006;12:6716.
10. Shin D, Vigneswaran N, Gillenwater A, Richards-Kortum R. Advances in fluorescence imaging techniques to detect oral cancer and its precursors. *Future Oncol.* 2010;6:1143–54.
11. Kois JC, Truelove E. Detecting oral cancer: a new technique and case reports. *Dent Today.* 2006;25:96–7.
12. Shashidara R, Sreeshyla HS, Sudheendra US. Chemiluminescence: A diagnostic adjunct in oral precancer and cancer: a review. *J Cancer Res Ther.* 2014;10:487–91.
13. Ram S, Siar CH. Chemiluminescence as a diagnostic aid in the detection of oral cancer and potentially malignant epithelial lesions. *Int J OralMaxillofac Surg.* 2005;34:521–7.
14. Mojsa I, Kaczmarzyk T, Zaleska M, Stypulkowska J, Zapala-Pospiech A, Sadecki D. Value of the ViziLite plus system as a diagnostic aid in the early detection of oral cancer/premalignant epithelial lesions. *J Craniofac Surg.* 2012;23:e162–4.
15. Awan KH, Morgan PR, Warnakulasuriya S. Utility of chemiluminescence (ViziLite™) in the detection of oral potentially malignant disorders and benign keratosis. *J Oral Pathol Med.* 2011;40:541–4.
16. Nagi R, Reddy-Kantharaj YB, Rakesh N, Janardhan-Reddy S, Sahu S. Efficacy of light based detection systems for early detection of oral cancer and oral

- potentially malignant disorders: systematic review. *Med Oral Patol Oral Cir Bucal*. 2016;21:e447–55.
17. Kerr AR, Sirois DA, Epstein JB. Clinical evaluation of chemiluminescent lighting: an adjunct for oral mucosal examinations. *J Clin Dent*. 2006;17:59–63.
 18. Rajmohan M, Rao UK, Joshua E, Rajasekaran ST, Kannan R. Assessment of oral mucosa in normal, precancer and cancer using chemiluminescent illumination, toluidine blue supravital staining and oral exfoliative cytology. *J Oral Maxillofac Pathol*. 2012;16:325–9.
 19. McIntosh L, McCullough MJ, Farah CS. The assessment of diffused light illumination and acetic acid rinse (Microlux/DL) in the visualisation of oral mucosal lesions. *Oral Oncol*. 2009;45:e227–31.
 20. Ibrahim SS, Al-Attas SA, Darwish ZE, Amer HA, Hassan MH. Effectiveness of the Microlux/DL™ chemiluminescence device in screening of potentially malignant and malignant oral lesions. *Asian Pac J Cancer Prev*. 2014;15:6081–6.
 21. Roblyer D, Kurachi C, Stepanek V, Williams MD, El-Naggar AK, Lee JJ, et al. Objective detection and delineation of oral neoplasia using autofluorescence imaging. *Cancer Prev Res (Phila)*. 2009;2:423–31.
 22. Messadi DV, Younai FS, Liu HH, Guo G, Wang CY. The clinical effectiveness of reflectance optical spectroscopy for the in vivo diagnosis of oral lesions. *Int J Oral Sci*. 2014;6:162–7.
 23. Wilder-Smith P, Holtzman J, Epstein J, Le A. Optical diagnostics in the oral cavity: an overview. *Oral Dis*. 2010;16:717–28.
 24. Schwarz RA, Gao W, Weber CR, Kurachi C, Lee JJ, El-Naggar AK, et al. Noninvasive evaluation of oral lesions using depth-sensitive optical spectroscopy. *Cancer*. 2009;115:1669–79.
 25. Yang SW, Lee YS, Chang LC, Chien HP, Chen TA. Clinical appraisal of endoscopy with narrow-band imaging system in the evaluation and management of homogeneous oral leukoplakia. *ORL J OtorhinolaryngolRelat Spec*. 2012;74:102–9.
 26. Yang SW, Lee YS, Chang LC, Hwang CC, Chen TA. Diagnostic significance of narrow-band imaging for detecting high-grade dysplasia, carcinoma in situ, and carcinoma in oral leukoplakia. *Laryngoscope*. 2012;122:2754–61.
 27. Yang SW, Lee YS, Chang LC, Hwang CC, Chen TA. Use of endoscopy with narrow-band imaging system in detecting squamous cell carcinoma in oral chronic non-healing ulcers. *Clin Oral Investig*. 2014;18:949–59.
 28. Yang SW, Lee YS, Chang LC, Chien HP, Chen TA. Light sources used in evaluating oral leukoplakia: broadband white light versus narrowband imaging. *Int J Oral Maxillofac Surg*. 2013;42:693–701.
 29. Yang SW, Lee YS, Chang LC, Hwang CC, Luo CM, Chen TA. Use of endoscopy with narrow-band imaging system in evaluating oral leukoplakia. *Head Neck*. 2012;34:1015–22.
 30. Green B, Cobb AR, Brennan PA, Hopper C. Optical diagnostic techniques for use in lesions of the head and neck: review of the latest developments. *Br J Oral Maxillofac Surg*. 2014;52:675–80.
 31. Yang SW, Lee YS, Chang LC, Hwang CC, Luo CM, Chen TA. Clinical characteristics of narrow-band imaging of oral erythroplakia and its correlation with pathology. *BMC Cancer*. 2015;15:406.
 32. Ottaviani G, Gobbo M, Rupel K, D'Ambros M, Perinetti G, Di Lenarda R, et al. The diagnostic performance parameters of narrow band imaging: a preclinical and clinical study. *Oral Oncol*. 2016;60:130–6.
 33. Zhou H, Zhang J, Guo L, Nie J, Zhu C, Ma X. The value of narrow band imaging in diagnosis of head and neck cancer: a meta-analysis. *Sci Rep*. 2018;8:515.
 34. Vu A, Farah CS. Narrow band imaging: clinical applications in oral and oropharyngeal cancer. *Oral Dis*. 2016;22:383–90.
 35. Roblyer D, Richards-Kortum R, Sokolov K, El-Naggar AK, Williams MD, Kurachi C, et al. Multispectral optical imaging device for in vivo detection of oral neoplasia. *J Biomed Opt*. 2008;13:024019.
 36. Shibahara T, Yamamoto N, Yakushiji T, Nomura T, Sekine R, Muramatsu K. Narrow-band imaging system with magnifying endoscopy for early oral cancer. *Bull Tokyo Dent Coll*. 2014;55:87–94.
 37. Takano JH, Yakushiji T, Kamiyama I, Nomura T, Katakura A, Takano N, et al. Detecting early oral cancer: narrow band imaging system observation of the oral mucosa microvasculature. *Int J OralMaxillofac Surg*. 2010;39:208–13.
 38. Yang SW, Lee YS, Chang LC, Hsieh TY, Chen TA. Implications of morphologic patterns of intraepithelial microvasculature observed by narrow-band imaging system in cases of oral squamous cell carcinoma. *Oral Oncol*. 2013;49:86–92.
 39. Sato H, Inoue H, Ikeda H, Sato C, Onimaru M, Hayee B, et al. Utility of intrapapillary capillary loops seen on magnifying narrow-band imaging in estimating invasive depth of esophageal squamous cell carcinoma. *Endoscopy*. 2015;47:122–8.
 40. Lingen MW, Tampi MP, Urquhart O, Abt E, Agrawal N, Chaturvedi AK, et al. Adjuncts for the evaluation of potentially malignant disorders in the oral cavity: Diagnostic test accuracy systematic review and meta-analysis—a report of the American Dental Association. *J Am Dent Assoc*. 2017;148:797–813.e52.
 41. Wang LV, Hu S. Photoacoustic tomography: in vivo imaging from organelles to organs. *Science*. 2012;335:1458–62.
 42. Bell AG. On the production and reproduction of sound by light. *Am J Sci*. 1880;118:305–24.
 43. Bowen T, Nasoni RL, Pifer AE, Sembroski GH. Some experimental results on the thermoacoustic imaging of tissue equivalent phantom materials. *Ultrasonics Symposium*. 1981:823–7.
 44. Bowen T. Radiation-induced thermoacoustic soft tissue imaging. *Ultrasonics Symposium*. 1981:817–22.
 45. Bowen T, Nasoni RL, Pifer AE. Thermoacoustic imaging induced by deeply penetrating radiation. *Acoustical Imaging*. 1984;13:409–27.

46. Kruger RA. Photoacoustic ultrasound. *Med Phys*. 1994;21:127–31.
47. Kruger RA, Liu P, Appledorn CR. Photoacoustic ultrasound (PAUS)—reconstruction tomography. *Med Phys*. 1995;22:1605–9.
48. Xu M, Wang LV. Photoacoustic imaging in biomedicine. *Rev Sci Instrum*. 2006;77:041101.
49. Valluru KS, Chinni B K, Rao N A, Bhatt S, Dogra, V S. Basics and clinical applications of photoacoustic imaging. *Ultrasound Clinics* 2009; 4 , 403–429.
50. Zhou Y, Wang D, Zhang Y, Chitgupi U, Geng J, Wang Y, et al. A phosphorus phthalocyanine formulation with intense absorbance at 1000 nm for deep optical imaging. *Theranostics*. 2016;6:688–97.
51. Li C, Wang LV. Photoacoustic tomography and sensing in biomedicine. *Phys Med Biol*. 2009;54:R59–97.
52. Kolkman R G, Hondebrink E, Steenbergen W, Mul F. In vivo photoacoustic imaging of blood vessels using an extreme-narrow aperture sensor. *IEEE J Selected Topics Quantum Electronics*. 2003;9:343–6.
53. Laufer J, Delpy D, Elwell C, Beard P. Quantitative spatially resolved measurement of tissue chromophore concentrations using photoacoustic spectroscopy: application to the measurement of blood oxygenation and haemoglobin concentration. *Phys Med Biol*. 2007;52:141–68.
54. Needles A, Heinmiller A, Sun J, Theodoropoulos C, Bates D, Hirson D, et al. Development and initial application of a fully integrated photoacoustic micro-ultrasound system. *IEEE Trans Ultrason Ferroelectr Freq Control*. 2013;60:888–97.
55. Beard P. Biomedical photoacoustic imaging. *Interface Focus*. 2011;1:602–31.
56. Lakshman M, Needles A. Screening and quantification of the tumor microenvironment with micro-ultrasound and photoacoustic imaging. *Nat Methods*. 2015;2015:12.
57. Liu Q. Role of optical spectroscopy using endogenous contrasts in clinical cancer diagnosis. *World J Clin Oncol*. 2011;2:50–63.
58. Yao DK, Maslov K, Shung KK, Zhou Q, Wang LV. In vivo label-free photoacoustic microscopy of cell nuclei by excitation of DNA and RNA. *Opt Lett*. 2010;35:4139–41.
59. Smith B D, Smith GL, Carter, D, Sasaki C T, Haffty B G. Prognostic significance of vascular endothelial growth factor protein levels in oral and oropharyngeal squamous cell carcinoma. *J Clin Oncol* 2000; 18: 2046–2052.
60. Brennan PA, Mackenzie N, Quintero M. Hypoxia-inducible factor 1 α in oral cancer. *J Oral Pathol Med*. 2005;34:385–9.
61. Oraevsky AA, Karabutov AA, Savateeva EV, Bell BA, Motamedi M, Thomsen SL, et al. Photoacoustic imaging of oral cancer: Feasibility studies in hamster model of squamous cell carcinoma. In *BiOS'99 International Biomedical Optics Symposium*; 1999. International Society for Optics and Photonics, pp. 385–396.
62. Savateeva EV, Karabutov AA, Motamedi M, Bell BA, Johnigan RM, Oraevsky AA. Noninvasive detection and staging of oral cancer in vivo with confocal photoacoustic tomography. In *BiOS 2000 the international symposium on biomedical optics*; 2000. International Society for Optics and Photonics. pp. 55–66.
63. Fatakawala H, Poti S, Zhou F, Sun Y, Bec J, Liu J, et al. Multimodal in vivo imaging of oral cancer using fluorescence lifetime, photoacoustic and ultrasound techniques. *Biomed Opt Express*. 2013;4:1724–41.
64. Dogra VS, Chinni BK, Valluru KS, Moalem J, Giampoli EJ, Evans K, et al. Preliminary results of ex vivo multispectral photoacoustic imaging in the management of thyroid cancer. *Am J Roentgenol*. 2014;202:W552–8.
65. Kima J, Kimb MH, Job K, Hab J, Kima Y, Limb DJ et al. Photoacoustic analysis of thyroid cancer in vivo: a pilot study. In *Proc. of SPIE Vol 2017, March*. (Vol. 10064, pp. 1006408–1).
66. Rich LJ, Seshadri M. Photoacoustic imaging of vascular hemodynamics: validation with blood oxygenation level–dependent MR imaging. *Radiology*. 2015;275:110–8.
67. Rich LJ, Seshadri M. Photoacoustic monitoring of tumor and normal tissue response to radiation. *Sci Rep*. 2016;6:21237.
68. Mallidi S, Watanabe K, Timmerman D, Schoenfeld D, Hasan T. Prediction of tumor recurrence and therapy monitoring using ultrasound-guided photoacoustic imaging. *Theranostics*. 2015;5:289–301.
69. Luke GP, Yeager D, Emelianov SY. Biomedical applications of photoacoustic imaging with exogenous contrast agents. *Ann Biomed Eng*. 2012;40:422–37.
70. Weber J, Beard PC, Bohndiek SE. Contrast agents for molecular photoacoustic imaging. *Nat Methods*. 2016;13:639–50.
71. Emelianov SY, Li PC, O'Donnell M. Photoacoustics for molecular imaging and therapy. *Phys Today*. 2009;62:34–9.
72. Li W, Chen X. Gold nanoparticles for photoacoustic imaging. *Nanomedicine (Lond)*. 2015;10:299–320.
73. Pan D, Kim B, Wang LV, Lanza GM. A brief account of nanoparticle contrast agents for photoacoustic imaging. *Wiley Interdiscip Rev Nanomed Nanobiotechnol*. 2013;5:517–43.
74. Mallidi S, Larson T, Tam J, Joshi PP, Karpouk A, Sokolov K, Emelianov S. Multiwavelength photoacoustic imaging and plasmon resonance coupling of gold nanoparticles for selective detection of cancer. *Nano Lett*. 2009;9:2825–31.
75. Nie L, Chen M, Sun X, Rong P, Zheng N, Chen X. Palladium nanosheets as highly stable and effective contrast agents for in vivo photoacoustic molecular imaging. *Nanoscale*. 2014;6:1271–6.
76. Li PC, Wang CR, Shieh DB, Wei CW, Liao CK, Poe C, et al. In vivo photoacoustic molecular imaging with simultaneous multiple selective targeting using antibody-conjugated gold nanorods. *Opt Express*. 2008;16:18605–15.
77. Chen YS, Frey W, Kim S, Homan K, Kruijzinga P, Sokolov K, et al. Enhanced thermal stability of silica-coated gold nanorods for photoacoustic

- imaging and image-guided therapy. *Opt Express*. 2010;18:8867–78.
78. Chen YS, Frey W, Kim S, Kruizinga P, Homan K, Emelianov S. Silica-coated gold nanorods as photoacoustic signal nanoamplifiers. *Nano Lett*. 2011;11:348–54.
 79. Garcia-Uribe A, Erpelding TN, Krumholz A, Ke H, Maslov K, Appleton C, et al. Dual-modality photoacoustic and ultrasound imaging system for noninvasive sentinel lymph node detection in patients with breast cancer. *Sci Rep*. 2015;5:15748.
 80. Stoffels I, Morscher S, Helfrich I, Hillen U, Leyh J, Burton NC, et al. Metastatic status of sentinel lymph nodes in melanoma determined noninvasively with multispectral optoacoustic imaging. *Sci Transl Med*. 2015;7:317ra199.
 81. Huynh E, Lovell J, Helfield BL, Jeon M, Kim C, Goertz DE, et al. Porphyrin shell microbubbles with intrinsic ultrasound and photoacoustic properties. *J Am Chem Soc*. 2012;134:16464–7.
 82. Muhanna N, Jin CS, Huynh E, Chan H, Qiu Y, Jiang W, et al. Phototheranostic porphyrin nanoparticles enable visualization and targeted treatment of head and neck cancer in clinically relevant models. *Theranostics*. 2015;5:1428–43.
 83. Yang Q, Cui H, Cai S, Yang X, Forrest ML. In vivo photoacoustic imaging of chemotherapy-induced apoptosis in squamous cell carcinoma using a near-infrared caspase-9 probe. *J Biomed Opt*. 2011;16:116026.
 84. Luke GP, Myers JN, Emelianov SY, Sokolov KV. Sentinel lymph node biopsy revisited: ultrasound-guided photoacoustic detection of micrometastases using molecularly targeted plasmonic nanosensors. *Cancer Res*. 2014;74:5397–408.
 85. Shakiba M, Ng KK, Huynh E, Chan H, Charron DM, Chen J, et al. Stable J-aggregation enabled dual photoacoustic and fluorescence nanoparticles for intraoperative cancer imaging. *Nanoscale*. 2016;8:12618.
 86. Luke GP, Emelianov SY. Label-free detection of lymph node metastases with US-guided functional photoacoustic imaging. *Radiology*. 2015;277:435–42.